Nakazawa et al. *NPG Asia Materials* (2024)16:57
https://doi.org/10.1038/s41427-024-00577-1

NPG Asia Materials

ARTICLE Open Access

Structure-dynamics relation in metallic glass revealed by 5-dimensional scanning transmission electron microscopy

Katsuaki Nakazawa[1], Kazutaka Mitsuishi[2], Konstantin Iakoubovskii[3], Shinji Kohara[2] and Koichi Tsuchiya[1,4]

Abstract

Dynamical and structural heterogeneities play an important role in glass transition phenomena. However, the relation between these heterogeneities is not fully revealed. In this study, we simultaneously observed these heterogeneities near the glass transition temperature in $Zr_{50}Cu_{40}Al_{10}$ using five-dimensional scanning transmission electron microscopy, which can record the spatiotemporal distribution of diffraction patterns. The heterogeneities were visualized with sub-nanometer resolution, and a correlation between them was measured up to the glass transition temperature. We verified that ordered structures had slow dynamics, and the order decreased as the temperature increased.

Introduction

Glass transition is a universal phenomenon observed in a wide range of materials, including metals, polymers, and ceramics, which were cooled from the melt quickly enough to avoid crystallization and freeze the constituent atoms or molecules in disordered positions[1,2]. Since the glass phase has different physical properties compared with a liquid or a crystal, and the glass transition is strongly related to crystallization and melting, this phenomenon is important for controlling physical and technological properties such as moldability[3]. However, the process of freezing the atomic dynamics is still not understood. In the glass transition phenomenon, the viscosity changes rapidly near the glass transition temperature (T_g), even though the *average* structure remains almost unchanged[4]. Hence, to explain the viscosity variations, researchers focused on the *microscopic* structure of glasses and supercooled liquids. Dynamical heterogeneity was discovered in simulations and experiments on colloidal systems[5,6], in which the motion of particles is heterogeneous and results in clustering. The dynamical heterogeneity shows a divergent behavior near T_g and is expected to explain the drastic change in viscosity during the glass transition. Furthermore, it has been revealed by electron tomography and other methods that there is a spatial heterogeneity of atomic arrangement in glasses[7–11]. This heterogeneity is called structural heterogeneity. The relation between dynamical and structural heterogeneities is important. If a common atomic structure of the slow-dynamics region in the dynamical heterogeneity is detected, it may become possible to identify the structures that cause the slow dynamics (high viscosity) and are necessary for the glass transition. Since atomic motion is affected by the surrounding atomic structure, there must be a relation between them. In fact, the relation between the structure and the temperature dependence of viscosity (fragility) has already been reported[12,13], and a relation between heterogeneities has been suggested,[14–18] but has not been confirmed experimentally so far, possibly because of the scarcity lack of observation methods that can simultaneously probe both the structural and dynamical heterogeneities. Those methods require a spatial resolution of a few nanometers, a time resolution of a few seconds, and the ability to measure the local structure of glass.

Correspondence: Katsuaki Nakazawa (NAKAZAWA.Katsuaki@nims.go.jp)
[1]International Center for Young Scientists, National Institute for Materials Science, 1-2-1, Sengen, Tsukuba, Ibaraki 305-0047, Japan
[2]Center for Basic Research on Materials, National Institute for Materials Science, 1-2-1, Sengen, Tsukuba, Ibaraki 305-0047, Japan
Full list of author information is available at the end of the article

Experimental methods for characterizing dynamics at the atomic scale in glass began with measuring average values using X-ray photon correlation microscopy (XPCS)[19–21], progressed to probing local dynamics with electron correlation microscopy (ECM)[22,23], and advanced to visualizing dynamical heterogeneities using dark-field electron correlation microscopy (DF-ECM)[24]. These methods did contribute to the understanding of glass dynamics, but they suffered from low spatial resolution (XPCS), inabilities to observe the spatial distribution (ECM) or local structures (DF-ECM). However, a novel technique of 5-dimensional scanning transmission electron microscopy (5D-STEM)[25–27] that involves convergent electron beam diffraction (CBED) does meet the requirements mentioned above. 5D-STEM is an extension of 4D-STEM[28]. It consists of 2D real-space scanning and 2D diffraction patterns, with the addition of a time dimension, and enables the measurement of the spatio-temporal distribution of CBED patterns. These patterns can yield local information that is hard to retrieve in the conventional parallel-beam diffraction mode. When a parallel electron beam irradiates a macroscale volume of a glass, a halo pattern is observed. However, when the probed volume shrinks to the nanoscale, intensity fluctuations, called speckles, appear instead[29,30]. The speckle pattern reflects the local order of the atomic structure[31–34], and its temporal change reflects the motion of the local atomic structure[22]. Thus, as illustrated in Fig. 1, the local structure of a glass can be analyzed from the spatial distribution of diffraction patterns, and the local atomic rearrangement can be measured from the corresponding time sequences.

In this study, we used 5D-STEM to simultaneously observe dynamical and structural heterogeneities and analyze the relation between them in a $Zr_{50}Cu_{40}Al_{10}$ metallic glass. We also conducted an in situ heating experiment to measure the temperature dependences of the dynamical and structural heterogeneities and the structure-dynamics relation below T_g.

Materials and methods

$Zr_{50}Cu_{40}Al_{10}$ metallic glass was fabricated by the tilt-melting method. Its glass transition and crystallization temperatures were 673 K and 750 K at the heating rate of 1.4 min/K[35]. TEM samples were fabricated by focused ion beam milling. STEM observation was conducted at 200 kV in an aberration-corrected JEM-ARM200F microscope (JEOL. Ltd.) equipped with a cold field emission gun and a 4DCanvas camera (JEOL. Ltd.). In the normal operation condition, the convergence semi-angle of the electron probe was in the range of 10 to 30 mrad (which corresponds to 6.0 to 18.0 nm^{-1}). This value is much larger than the typical diffraction angle of speckles, and hence it was not possible to observe them. Therefore, the condenser lens and one of the transfer lenses of the corrector were adjusted to achieve an appropriate convergence semi-angle of 1.6 mrad (0.95 nm^{-1}) that results in a probe diameter of 0.78 nm (full width at half maximum). The probe current was 8.9 pA. We used a beam stop to save the detector from the transmitted electron beam. The shadow of the beam stop was excluded from the analysis by excluding this area from the calculation of eqs. (1) and (5). To investigate temperature dependences of dynamical and structural heterogeneities and structure-dynamics relations, we heated the sample from 633 to 673 K in 10 K increments. Each diffraction pattern was acquired within 1 ms at 633 and 643 K and within 0.5 ms at 653, 663, and 673 K. The number of scan points and the step were 60 × 120 and 0.16 nm, respectively. The total observation area was 9.7 × 19.4 nm. Since 5D-STEM requires a sample edge for data calibration, we set the observation area as a horizontal rectangle. A total of 106 diffraction patterns were acquired for each scan point with a 9.2 s time resolution at 633 and 643 K and a 4.8 s time resolution at 653, 663, and 673 K. The total observation time was 1048 s at 633 and 643 K and 524 s at 653, 663, and 673 K. The pixel size and number of pixels for diffraction patterns were 0.058 nm^{-1} and 264 × 264. The diffraction patterns were 4 × 4 binned to increase the signal-to-noise ratio. The resultant pixel size and the number of pixels were 0.23 nm^{-1} and 66 × 66. The diffraction patterns near the sample edge (the left part of the sample) were too noisy for reliable measurements because of their thin thickness. Therefore, we used only the right half of the observed area whose thickness range is 40–50 nm in this article (see Fig. S1) to reduce thickness dependence and eliminate spurious signals.

Results and discussion

The local dynamics were evaluated from the temporal change of the local diffraction patterns using the following equations:[16,20,21,36,37]

$$G(Q,t_1,t_2)=\frac{\langle I(\boldsymbol{Q},t_1)I(\boldsymbol{Q},t_2)\rangle_\phi}{\langle I(\boldsymbol{Q},t_1)\rangle_\phi\langle I(\boldsymbol{Q},t_2)\rangle_\phi} \quad (1)$$

$$g(Q,t)=\langle G(Q,t_1,t)\rangle_{t_1} \quad (2)$$

Here $\boldsymbol{Q}$ is the position vector in reciprocal space, its absolute value Q is the spatial frequency and t, t_1 and t_2 are acquisition times. $G(Q,t_1,t_2)$ measures the correlation between diffractions acquired at times t_1 and t_2. $I(\boldsymbol{Q},t_1)$ is the signal intensity at $\boldsymbol{Q}$ and t_1, and $\langle\cdots\rangle_\phi$ the subscript ϕ indicates that the averaging is performed on the ensemble of pixels over a range of spatial frequency. In this study, we limited the frequency to the range of 4.2–4.6 nm^{-1} that covered the first sharp diffraction peaks. Strong speckles are observed when the electron beam irradiates an ordered atomic structure along its symmetry axis. Speckles are formed when the electron beam irradiates an ordered atomic structure along its

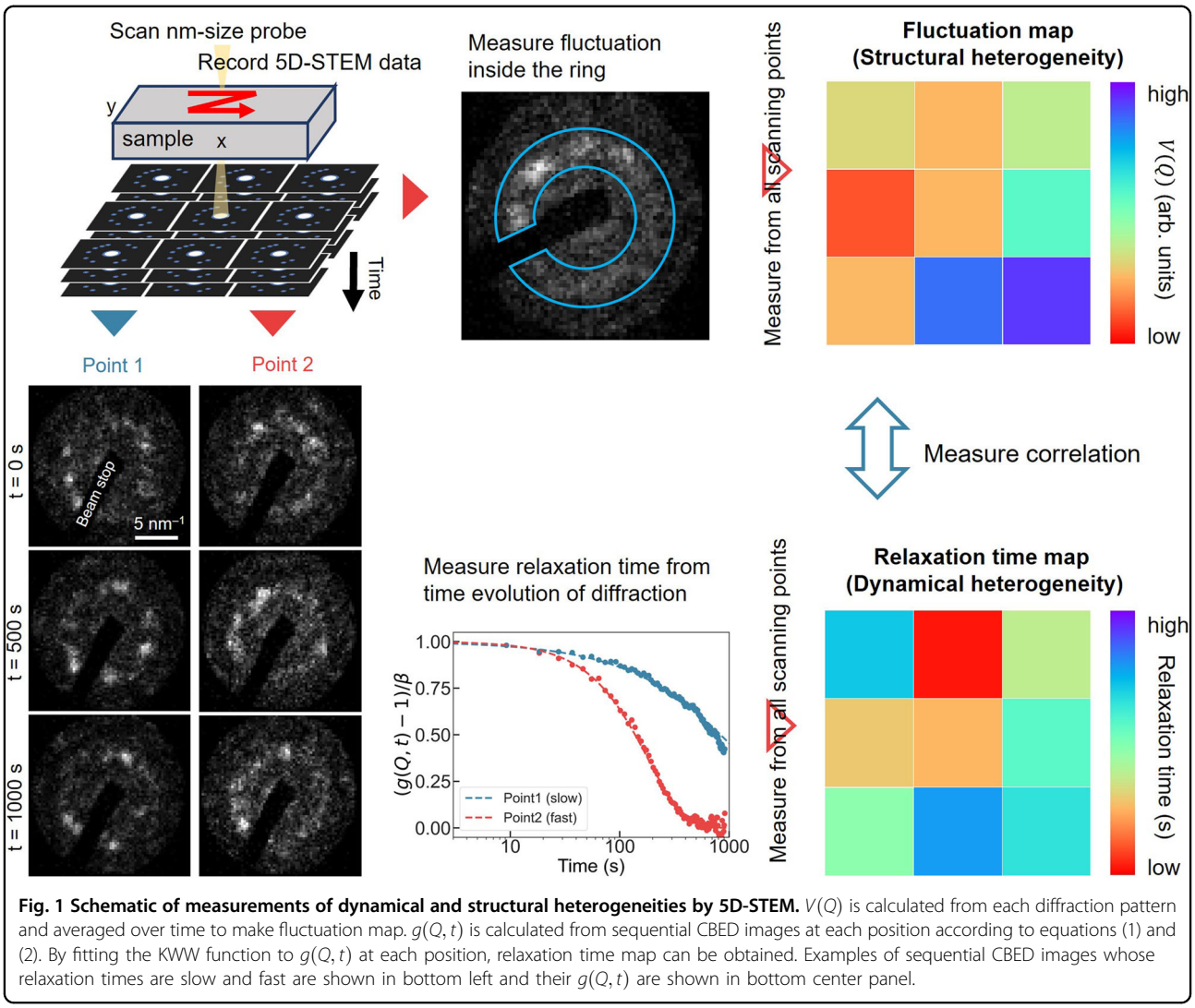

Fig. 1 Schematic of measurements of dynamical and structural heterogeneities by 5D-STEM. $V(Q)$ is calculated from each diffraction pattern and averaged over time to make fluctuation map. $g(Q,t)$ is calculated from sequential CBED images at each position according to equations (1) and (2). By fitting the KWW function to $g(Q,t)$ at each position, relaxation time map can be obtained. Examples of sequential CBED images whose relaxation times are slow and fast are shown in bottom left and their $g(Q,t)$ are shown in bottom center panel.

symmetry axis. Thus, this method probes the dynamics of the ordered atomic structures whose crystal symmetry axis is aligned to the beam direction. $g(Q,t)$ takes the average of $G(Q,t_1,t_2)$ over t_1, at a fixed delay time, $t = t_2 - t_1$. The Kohlrausch-Williams-Watts (KWW) function was fitted to $g(Q,t)$ to measure the dynamics.

$$g(Q,t) - 1 = \beta \exp\left(-2\left(\frac{t}{\tau}\right)^{\gamma}\right) \quad (3)$$

Here β, τ and γ are a scaling constant, the relaxation time, and the stretch factor, respectively. The stretch factor represents the nonlinearity of relaxation and indicates whether relaxation is compressed (γ>1) or stretched (γ<1) as compared to the simple exponent. Relaxation time is an indicator of dynamics; long relaxation time indicates slow dynamics and vice versa. We measured the relaxation time from all scan points to obtain a relaxation time map that directly reflects the dynamical heterogeneity. The relaxation time map for 633 K is presented in Fig. 2a. As seen from the map, the relaxation time spatially varies from 200 s to 5000 s revealing a heterogeneity of local dynamics. As shown in Fig. 2b–e, although the relaxation times vary, the dynamical heterogeneity has been observed at different temperatures. The average relaxation time is plotted in Fig. 2f; it shortens as the temperature approaches T_g, indicating an increase in atomic mobility. These values show good agreement with the previous research of Zr–Cu–Al systems, and such temperature dependence was observed in a series of metallic glasses using various measuring methods[38–40]. In samples with similar composition ($Cu_{59}Zr_{41}$), the relaxation process below T_g is thought of as β-relaxation. From the energy landscape perspective, β-relaxation is recognized as hopping across sub-basins inside an identical mega-basin. The activation energy to cross the sub-basins can be estimated from the temperature dependence of the relaxation time below T_g. The relation between relaxation time and activation energy is

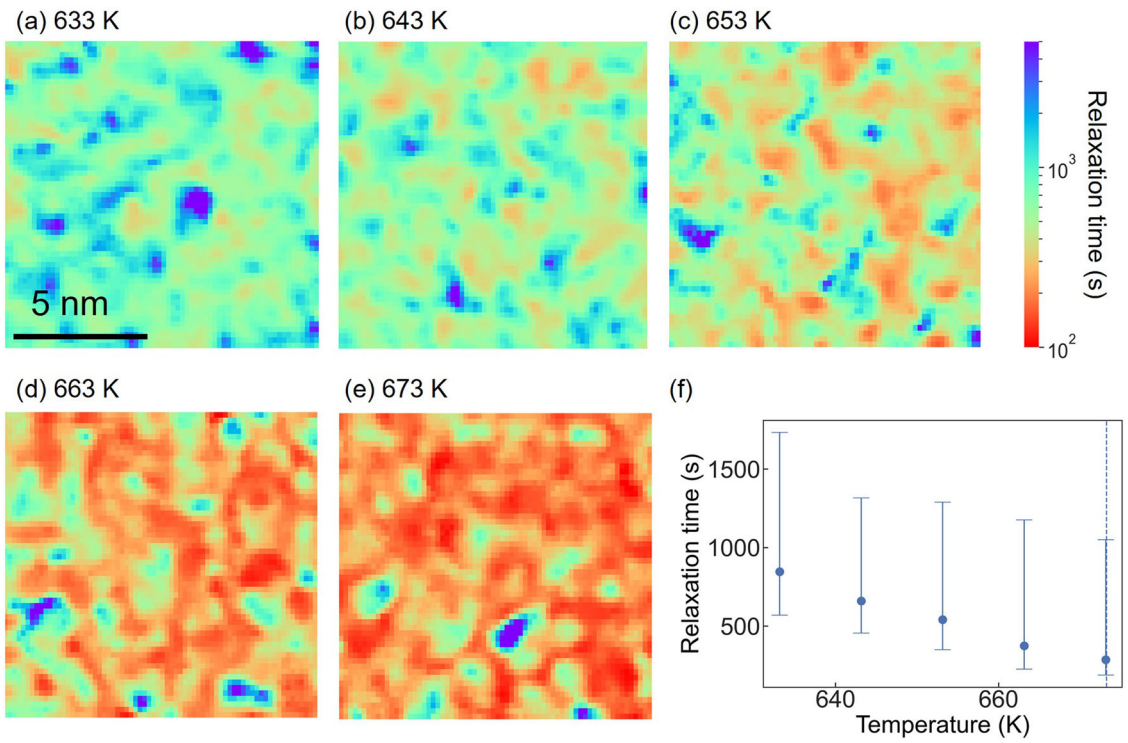

Fig. 2 Visualized dynamical heterogeneities. Maps of relaxation time at **a** 633 K, **b** 643 K, **c** 653 K, **d** 663 K, and **e** 673 K. **f** Temperature dependence of the spatially averaged relaxation time. The error bar shows the distribution of relaxation time.

expressed by the Arrhenius law.

$$\tau = \tau_\infty \exp\left(\frac{E_\beta}{RT}\right), \tag{4}$$

Where τ_∞ is the relaxation time at infinite temperature, E_β is the activation energy and R is the gas constant. The activation energy was calculated as 97 ± kJ/mol. This value falls within the range of the previously reported values, namely, 46 kJ/mol by internal friction measurements in $Cu_{59}Zr_{41}$[41], 96–159 kJ/mol by MD simulations of the Zr-Cu system[42–44], and 62–174 kJ/mol by dynamic mechanical analysis of Zr-Cu-Al alloys[45–47].

To evaluate the structural heterogeneity, we measured the intensity fluctuation along the azimuthal direction around the halo pattern. This intensity fluctuation mainly originates from the speckle pattern. The fluctuation is evaluated by the following equation:

$$V(Q,\boldsymbol{r}) = \frac{\langle I(\boldsymbol{Q},\boldsymbol{r})^2\rangle_\phi}{\langle I(\boldsymbol{Q},\boldsymbol{r})\rangle_\phi^2} - 1 \tag{5}$$

Since the speckle pattern reflects the local atomic structure, so does the value of $V(Q,\boldsymbol{r})$—a higher $V(Q,\boldsymbol{r})$ corresponds to a more ordered structure[32,48]. It should be noted that the value of $V(Q,\boldsymbol{r})$ is also influenced by the direction of the symmetry axis. However, since glass is isotropic, such effects can be greatly reduced by statistical sampling, making $V(Q,\boldsymbol{r})$ a reliable indicator for measuring overall trends and correlations. In this experiment, $V(Q,\boldsymbol{r})$ was measured from diffractions whose spatial frequency ranged from 3.0 to 5.8 nm^{-1}. We measured $V(Q,\boldsymbol{r})$ for all scanning points and averaged it over time. Figure 3a shows the calculated fluctuation map at 633 K. The values range from 0.45 to 0.75 and show heterogeneous distribution, indicating the coexistence of different local atomic structures. This image directly visualizes the structural heterogeneity of metallic glass. Thus, it was confirmed that the local atomic structure was heterogeneous. As shown in Fig. 3b–e, although the $V(Q,\boldsymbol{r})$ values vary, the structural heterogeneity has been observed at different temperatures. The temperature dependence of average $V(Q,\boldsymbol{r})$ is shown in Fig. 3f. The average $V(Q,\boldsymbol{r})$ slightly decreased with temperature from 0.56 to 0.52, reflecting the decrease in atomic order. A similar slight decrease in the average local order was theoretically predicted for $Zr_{47.5}Cu_{47.5}Al_5$ glass[49].

As mentioned above, the dynamical and structural heterogeneities can be measured simultaneously by 5D-STEM. The structure-dynamics relation was evaluated from these heterogeneities by correlating the maps of relaxation time and $V(Q,\boldsymbol{r})$. Since the local order was

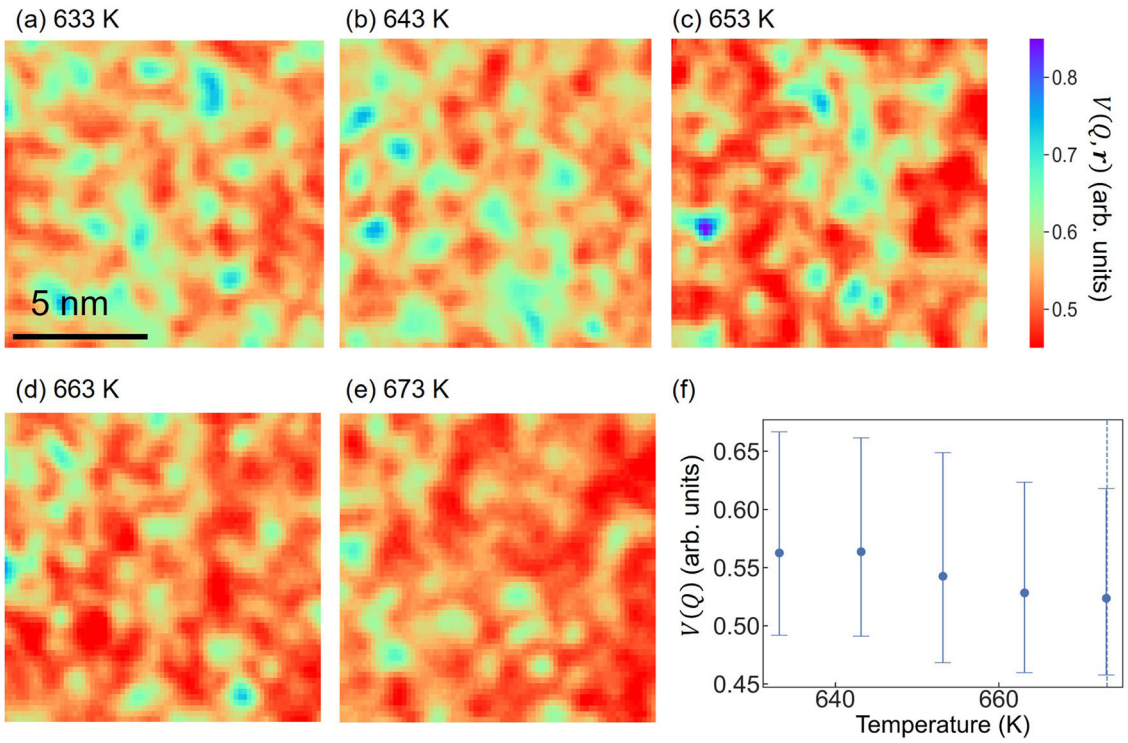

Fig. 3 Visualized structural heterogeneities. Maps of $V(Q, \boldsymbol{r})$ at **a** 633 K, **b** 643 K, **c** 653 K, **d** 663 K, and **e** 673 K. **f** The average $V(Q)$ at all temperatures. The errorbar shows the distribution of $V(Q)$. Q is the spatial frequency and ranged from 3.0 to 5.8 nm^{-1} in this calculation.

probed by the speckle pattern and the local relaxation time was measured from the temporal change of the same pattern, the local atomic order and atomic rearrangements were measured from the same nanostructure, and the correlation between dynamical and structural heterogeneities directly reflects the structure-dynamic relation. The degree of relaxation depends both on the relaxation time and the value of γ[50]. To simplify the analysis, considering that γ values are close to 1 (see Figs. S1 and S2), we fixed γ at 1.0. The correlation was calculated by Spearman's rank correlation, where the correlation value can range from −1 to 1. Positive and negative values mean positive and negative correlations between the maps of relaxation time and $V(Q, \boldsymbol{r})$, while 0 means lack of correlation. A scatter plot is shown in Fig. 4 with $V(Q, \boldsymbol{r})$ on the vertical axis and relaxation time on the horizontal axis. At 633 K, the distribution of the points is stretched from the center to the upper right, and the correlation value is 0.39, statistically indicating that regions with a long relaxation time and regions with a partial order tend to coincide. Thus, ordered regions tend to have slow dynamics. This tendency is also observed in simulations of polydisperse particles[14]. It is noteworthy that not all structural heterogeneities exhibit correlations with dynamical heterogeneities. Structural heterogeneities calculated by density or potential energy fields do not exhibit a positive correlation with dynamical heterogeneities[14,51]. Simulation studies have demonstrated that the multi-body effects such as flexibility[17], deviations from sterically favored structures[14], or softness[18] are significant in explaining dynamical heterogeneity, as the relaxation process is affected by surrounding atoms or particles. The diffraction or speckle pattern formed by the interference of electrons scattered by atoms naturally includes information about surrounding atoms[31]. Therefore, a positive correlation has been observed between structural heterogeneity measured by $V(Q)$ and dynamical heterogeneity. The same tendency is observed at higher temperatures, as shown in Fig. 4b–e, and especially in Fig. 4f, which superimposes the scatter plots for all temperatures. Figure 4f reveals that the relaxation time shortens at higher temperatures. Meanwhile, the shift in the distribution toward the lower left corner indicates that the number of less regular structures that exhibit higher atomic mobility increases at high temperatures.

In summary, our results can be interpreted as follows: at low temperatures, the atomic rearrangement was slow. As the temperature increased, the atomic motion sped up, and the degree of local atomic order decreased. The atomic motion was slow for ordered regions regardless of temperature. The atomic motion accelerated near T_g for two reasons: (1) an increase in the number of structures

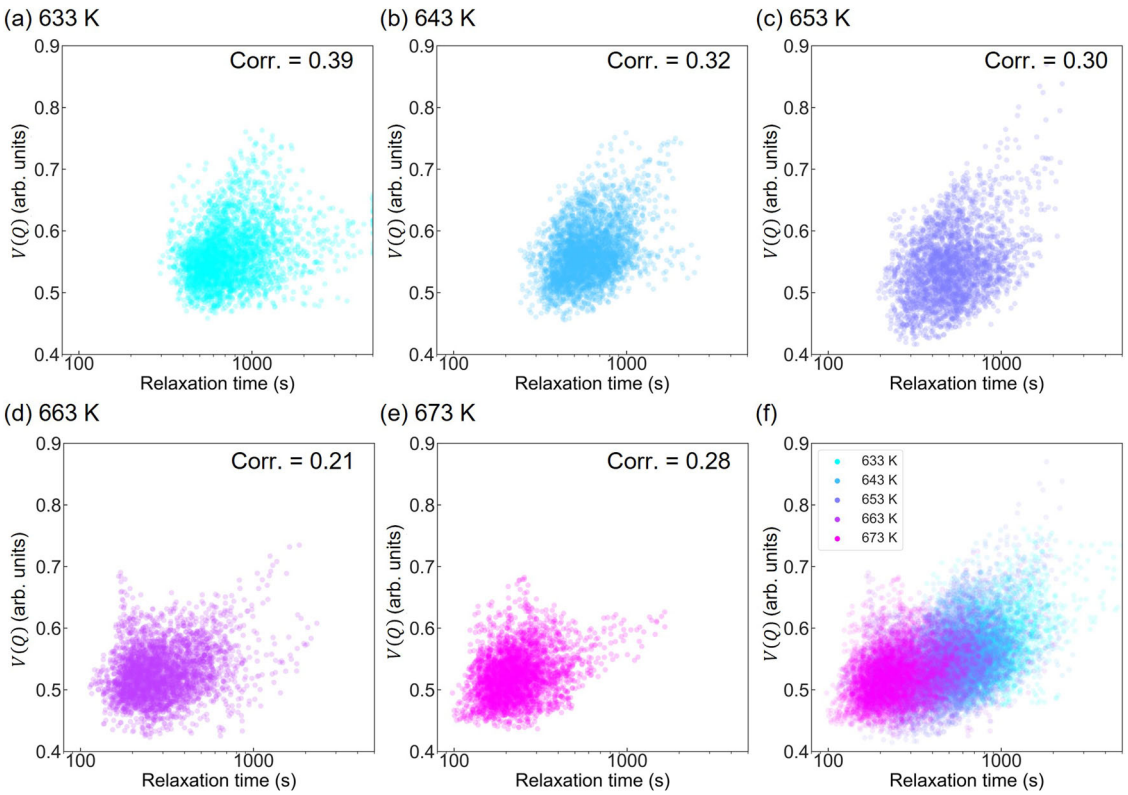

Fig. 4 Correlation between dynamical and structural heterogeneities. Scatter plots of relaxation time and $V(Q)$ at **a** 633 K, **b** 643 K, **c** 653 K, **d** 663 K, **e** 673 K. **f** Superimposed scatter plots at all temperatures.

that have a low degree of order and hence a high atomic mobility, and (2) an increase in the atomic mobility in structures with any degree of order.

Structural and dynamical heterogeneities are important for elucidating the mechanism of glass transition. However, the relationship between these heterogeneities is difficult to analyze because of the lack of experimental methods that can simultaneously measure these heterogeneities. In this study, we simultaneously visualized the dynamical and structural heterogeneities in a $Zr_{50}Cu_{40}Al_{10}$ metallic glass by recording the spatio-temporal distribution of diffraction patterns via 5D-STEM. We also measured the temperature dependencies of relaxation time and structural order. The results directly reveal a positive correlation between dynamical and structural heterogeneities, indicating that atomic rearrangement is slower in more ordered atomic structures. This study demonstrates the high potential of 5D-STEM in monitoring the dynamical and structural heterogeneities in glasses, yet the reported calculation of $V(Q, \boldsymbol{r})$ can only hint at the presence of the ordered structure. Therefore, a better correlation of structure and dynamics would require the development of new analytical methods for diffraction patterns that can identify translational symmetry, rotational symmetry, and whether the structural order is energy-driven or entropy-driven, as proposed for atomic structures in real space[52].

Acknowledgements
We thank Ms. K. Shiomi for her help with the preparation of the sample and Prof. T. Sannomiya for advice on STEM electron optics. We also would like to thank Profs. T. Ichitsubo and H. Kato for fruitful discussions. This work was supported by JSPS KAKENHI Grant Number JP23K13076. This research is founded by JSPS KAKENHI Grant Number JP23K13076.

Author details
[1]International Center for Young Scientists, National Institute for Materials Science, 1-2-1, Sengen, Tsukuba, Ibaraki 305-0047, Japan. [2]Center for Basic Research on Materials, National Institute for Materials Science, 1-2-1, Sengen, Tsukuba, Ibaraki 305-0047, Japan. [3]Department of Physics, National University of Singapore, Singapore 117551, Singapore. [4]Research Center for Structural Materials, National Institute for Materials Science, 1-2-1, Sengen, Tsukuba, Ibaraki 305-0047, Japan

Author contributions
K.N., S.K., and K.M. conceived the idea and experiments. K.T. prepared bulk $Zr_{50}Cu_{40}Al_{10}$ metallic glass, and K.N. processed the TEM sample. K.N., K.M., and K.I. measured relaxation time. K.N. and K.I. analyzed the data and wrote the manuscript. K.N. and S.K. prepared the figures. All the authors participated in the manuscript review.

Conflict of interest
The authors declare no competing interests.

Supplementary information The online version contains supplementary material available at https://doi.org/10.1038/s41427-024-00577-1.

Received: 2 April 2024 Revised: 9 October 2024 Accepted: 14 October 2024
Published online: 15 November 2024

References

1. Angell, C. A. Perspective on the glass transition. *J. Phys. Chem. Solids* **49**, 863–871 (1988).
2. Berthier, L. & Biroli, G. Theoretical perspective on the glass transition and amorphous materials. *Rev. Mod. Phys.* **83**, 587–645 (2011).
3. Shintani, H. & Tanaka, H. Frustration on the way to crystallization in glass. *Nat. Phys.* **2**, 200–206 (2006).
4. Kauzmann, W. The nature of the glassy state and the behavior of liquids at low temperatures. *Chem. Rev.* **43**, 219–256 (1948).
5. Yamamoto, R. & Onuki, A. Dynamics of highly supercooled liquids: heterogeneity, rheology, and diffusion. *Phys. Rev. E* **58**, 3515–3529 (1998).
6. Weeks, E. R., Crocker, J. C., Levitt, A. C., Schofield, A. & Weitz, D. A. Three-dimensional direct imaging of structural relaxation near the colloidal glass transition. *Science* **287**, 627–631 (2000).
7. Yang, Y. et al. Determining the three-dimensional atomic structure of an amorphous solid. *Nature* **592**, 60–64 (2021).
8. Ichitsubo, T. et al. Microstructure of fragile metallic glasses inferred from ultrasound-accelerated crystallization in Pd-based metallic glasses. *Phys. Rev. Lett.* **95**, 245501 (2005).
9. Li, M., Wang, C. Z., Hao, S. G., Kramer, M. J. & Ho, K. M. Structural heterogeneity and medium-range order in Zr_xCu_{100-x} metallic glasses. *Phys. Rev. B* **80**, 184201 (2009).
10. Im, S. et al. J. Medium-range ordering, structural heterogeneity, and their influence on properties of Zr-Cu-Co-Al metallic glasses. *Phys. Rev. Mater.* **5**, 115604 (2021).
11. Zhao, P., Li, J., Hwang, J. & Wang, Y. Influence of nanoscale structural heterogeneity on shear banding in metallic glasses. *Acta Mater.* **134**, 104–115 (2017).
12. Kelton, K. F. Kinetic and structural fragility—a correlation between structures and dynamics in metallic liquids and glasses. *J. Phys. Conden. Matter* **29**, 023002 (2017).
13. Mauro, N. A., Blodgett, M., Johnson, M. L., Vogt, A. J. & Kelton, K. F. A structural signature of liquid fragility. *Nat. Commun.* **5**, 4616 (2014).
14. Tong, H. & Tanaka, H. Revealing hidden structural order controlling both fast and slow glassy dynamics in supercooled liquids. *Phys. Rev. X* **8**, 011041 (2018).
15. Zhu, F. et al. Intrinsic correlation between β-relaxation and spatial heterogeneity in a metallic glass. *Nat. Commun.* **7**, 11516 (2016).
16. Spangenberg, K., Hilke, S., Wilde, G. & Peterlechner, M. Direct view on non-equilibrium heterogeneous dynamics in glassy nanorods. *Adv. Funct. Mater.* **31**, 2103742 (2021).
17. Ding, J. et al. Universal structural parameter to quantitatively predict metallic glass properties. *Nat. Commun.* **7**, 13733 (2016).
18. Schoenholz, S. S., Cubuk, E. D., Sussman, D. M., Kaxiras, E. & Liu, A. J. A structural approach to relaxation in glassy liquids. *Nat. Phys.* **12**, 469–471 (2016).
19. Ruta, B. et al. Revealing the fast atomic motion of network glasses. *Nat. Commun.* **5**, 3939 (2014).
20. Evenson, Z. et al. X-ray photon correlation spectroscopy reveals intermittent aging dynamics in a metallic glass. *Phys. Rev. Lett.* **115**, 175701 (2015).
21. Das, A., Dufresne, E. M. & Maaß, R. Structural dynamics and rejuvenation during cryogenic cycling in a Zr-based metallic glass. *Acta Mater.* **196**, 723–732 (2020).
22. He, L., Zhang, P., Besser, M. F., Kramer, M. J. & Voyles, P. M. Electron correlation microscopy: a new technique for studying local atom dynamics applied to a supercooled liquid. *Micros. Microanal.* **21**, 1026–1033 (2015).
23. Zhang, P. et al. Applications and limitations of electron correlation microscopy to study relaxation dynamics in supercooled liquids. *Ultramicroscopy* **178**, 125–130 (2017).
24. Zhang, P., Maldonis, J. J., Liu, Z., Schroers, J. & Voyles, P. M. Spatially heterogeneous dynamics in a metallic glass forming liquid imaged by electron correlation microscopy. *Nat. Commun.* **9**, 1129 (2018).
25. Nakazawa, K. & Mitsuishi, K. Development of temporal series 4D-STEM and application to relaxation time measurement. *Microscopy* **72**, 446–449 (2023).
26. Mittelberger, A. et al. 5D-STEM: live processing and display at 15,000 diffraction patterns per second. *Micros. Microanal.* **27**, 1064–1065 (2021).
27. Nakamura, A., Shimojima, T. & Ishizaka, K. Visualizing optically-induced strains by five-dimensional ultrafast electron microscopy. *Faraday Discuss.* **237**, 27–39 (2022).
28. Ophus, C. Four-dimensional scanning transmission electron microscopy (4D-STEM): from scanning nanodiffraction to ptychography and beyond. *Micros. Microanal.* **25**, 563–582 (2019).
29. Voyles, P. M. & Muller, D. A. Fluctuation microscopy in the STEM. *Ultramicroscopy* **93**, 147–159 (2002).
30. Voyles, P. & Hwang, J. in *Characterization of Materials* (ed. Kaufmann, E. N.) (John Wiley & Sons, Inc., 2012).
31. Hirata, A. et al. Direct observation of local atomic order in a metallic glass. *Nat. Mater.* **10**, 28–33 (2011).
32. Hirata, A. & Chen, M. Angstrom-beam electron diffraction of amorphous materials. *J. Non-Cryst. Solids* **383**, 52–58 (2014).
33. Im, S. et al. Direct determination of structural heterogeneity in metallic glasses using four-dimensional scanning transmission electron microscopy. *Ultramicroscopy* **195**, 189–193 (2018).
34. Nakazawa, K. et al. Nanoscale strain mapping and symmetry analysis of $Zr_{50}Cu_{40}Al_{10}$ metallic glass rejuvenated by high-pressure torsion via 4D scanning transmission electron microscopy. *J. Non-Cryst. Solids* **606**, 122197 (2023).
35. Zhang, S. et al. Crystallization behavior and structural stability of $Zr_{50}Cu_{40}Al_{10}$ bulk metallic glass. *Mater. Trans.* **50**, 1340–1345 (2009).
36. Madsen, A., Leheny, R. L., Guo, H., Sprung, M. & Czakkel, O. Beyond simple exponential correlation functions and equilibrium dynamics in x-ray photon correlation spectroscopy. *N. J. Phys.* **12**, 055001 (2010).
37. Amini, N. et al. Intrinsic relaxation in a supercooled ZrTiNiCuBe glass forming liquid. *Phys. Rev. Mater.* **5**, 1–8 (2021).
38. Liu, C. et al. Sub-Tg relaxation times of the α process in metallic glasses. *J. Non-Cryst. Solids* **471**, 322–327 (2017).
39. Liu, C., Pineda, E. & Crespo, D. Characterization of mechanical relaxation in a Cu-Zr-Al metallic glass. *J. Alloy. Compd.* **643**, S17–S21 (2015).
40. Haruyama, O. et al. Characterization of free volume in cold-rolled $Zr_{55}Cu_{30}Ni_5Al_{10}$ bulk metallic glasses. *Acta Mater.* **61**, 3224–3232 (2013).
41. Deng, D. & Argon, A. S. Structural relaxation and embrittlement of $Cu_{59}Zr_{41}$ and $Fe_{80}B_{20}$ glasses. *Acta Metall.* **34**, 2011–2023 (1986).
42. Sun, Y. L., Shen, J. & Valladares, A. A. Atomic structure and diffusion in $Cu_{60}Zr_{40}$ metallic liquid and glass: Molecular dynamics simulations. *J. Appl. Phys.* **106**, 073520 (2009).
43. Annamareddy, A., Li, Y., Yu, L., Voyles, P. M. & Morgan, D. Factors correlating to enhanced surface diffusion in metallic glasses. *J. Chem. Phys.* **154**, 104502 (2021).
44. Annamareddy, A., Voyles, P. M., Perepezko, J. & Morgan, D. Mechanisms of bulk and surface diffusion in metallic glasses determined from molecular dynamics simulations. *Acta Mater.* **209**, 116794 (2021).
45. Pelletier, J. M., Yokoyama, Y. & Inoue, A. Dynamic mechanical properties in a $Zr_{50}Cu_{40}Al_{10}$ bulk metallic glass. *Mater. Trans.* **48**, 1359–1362 (2007).
46. Yu, H. B., Wang, W. H., Bai, H. Y., Wu, Y. & Chen, M. W. Relating activation of shear transformation zones to β relaxations in metallic glasses. *Phys. Rev. B* **81**, 220201 (2010).
47. Zhao, Z. F., Wen, P., Shek, C. H. & Wang, W. H. Measurements of slow β-relaxations in metallic glasses and supercooled liquids. *Phys. Rev. B* **75**, 174201 (2007).
48. Hirata, A. Local structure analysis of amorphous materials by angstrom-beam electron diffraction. *Microscopy* **70**, 171–177 (2021).
49. Wang, J. G., Chang, C. T., Song, K. K., Wang, L. & Pan, Y. Short-range ordering in metallic supercooled liquids and glasses. *J. Alloy. Compd.* **770**, 386–394 (2019).
50. Wu, J. H. & Jia, Q. The heterogeneous energy landscape expression of KWW relaxation. *Sci. Rep.* **6**, 20506 (2016).
51. Tanaka, H. Bond orientational order in liquids: Towards a unified description of water-like anomalies, liquid-liquid transition, glass transition, and crystallization: Bond orientational order in liquids. *Eur. Phys. J. E Soft Matter* **35**, 113 (2012).
52. Tanaka, H., Tong, H., Shi, R. & Russo, J. Revealing key structural features hidden in liquids and glasses. *Nat. Rev. Phys.* **1**, 333–348 (2019).